Fluid Inclusion Study of Gold Mineralization at the Taungzaw Area, Kanbalu Township, Sagaing Region, Myanmar

Aung Myo Kyaw[1] and Day Wa Aung[2]

Abstract

The Taungzaw area is located in Kanbalu Township, Sagaing Region, the Northern Myanmar. It lies in the eastern trough of the Central Myanmar Basin. Gold mineralization at the Taungzaw prospect occurs as a stockworks/dissemination style with localized breccia zones in silicified sandstone of the Eocene Male Formation. The mineralization appears to be closely associated with NNE-SSW trending extensional fault, which is probably related directly to the dextral movement of the Sagaing Fault system. Intense silicification associated with sericitization, argillic alteration, and decalcification is recognized in the ore zone. The gold grade is around 2.5 to 3g/t. The important ore minerals associated with gold mineralization are pyrite, chalcopyrite and arsenopyrite. Gold occurs as free particles or encapsulated with pyrite, chalcopyrite, arsenopyrite and tetrahedrite. Silver, copper, arsenic and antimony particularly appear to be good pathfinders and the best geochemical indicators of the gold mineralization. The fluid inclusion micro thermometric study indicates that the ore mineralization is characterized by the temperature of homogenization ranging from 162.2 and 256.3ºC and salinities ranging from 0.71 to 2.54wt.% NaCl equivalent. According to the fluid inclusion study, micro thermometry measurements and ore minerals assemblage and paleo-depth estimation, and hydrothermal alteration types of the Taungzaw prospect imply formation under an epithermal environment.

Keywords: Central Myanmar Basin, epithermal environment, Male Formation, Sagaing Fault, Taungzaw area

Introduction

The Taungzaw area is approximately 45km northeast of Kanbalu and 220km north of Mandalay. The study area is about 8 km long from north to south and 10 km wide from east to west, the total area coverage is about 80 square kilometers. It is about 10 km east of Mandalay-Myitkyina motorway and can be easily accessed throughout the whole year. The location map of the study area is shown in (Figure.1).

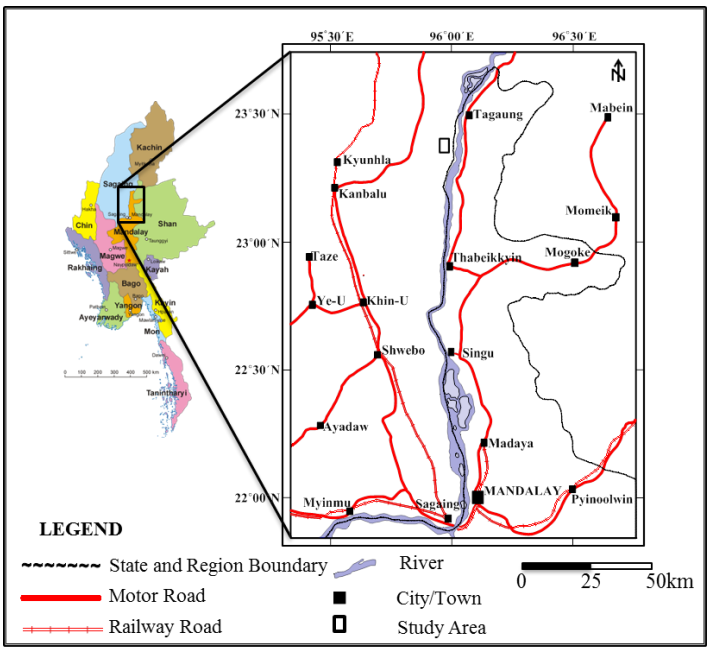

Figure (1): Location Map of the Study Area

[1] Lecturer, Science and Technology Research Center, Pyin Oo Lwin, Myanmar.

[2] Dr., Professor & Head, Department of Geology, University of Yangon, Myanmar.

This research attempts to provide the geological, mineralogical, and geochemical characteristics of gold mineralization in sedimentary rocks of the Taungzaw deposits. Some of the conclusions obtained from this study may be applicable to other similar epithermal deposits throughout the country. Taungzaw gold prospect belongs to one of the prominent sediment-hosted gold mineralization along the Sagaing Fault zone. The location of major gold deposits and the prospect of Myanmar is shown in (Fig.2).

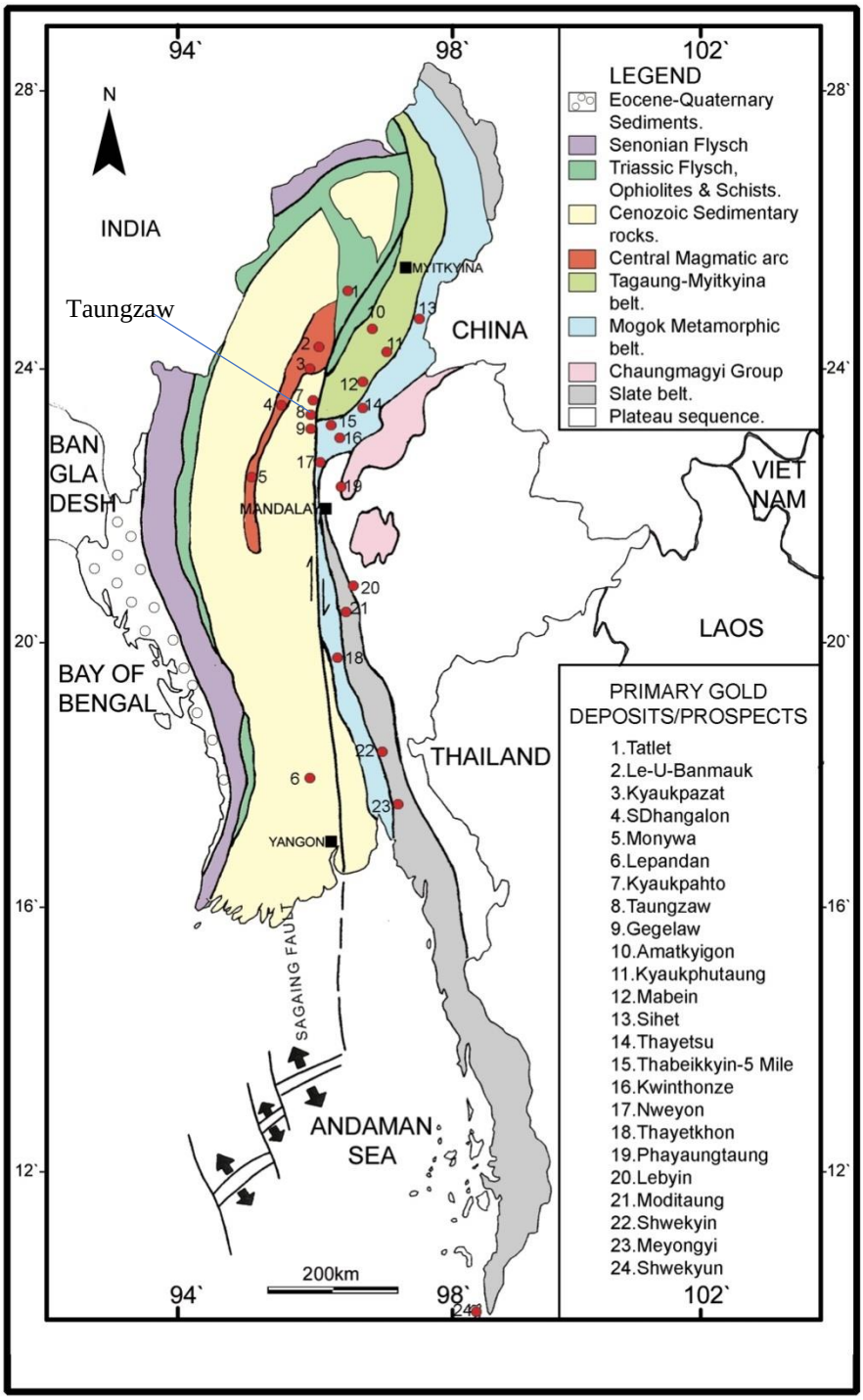

Figure (2): Major structural belts and location of major gold deposits and prospects in Myanmar. (simplified after, Mitchell,2004, Ye Myint Swe et.al,2004)

Regional Geology

The study area lies in the eastern Tertiary sedimentary basin of Myanmar and is located 2 km close to the west of the Sagaing Fault zone, a continental-scale right-lateral transform fault which marks the boundary between the West Burma continental plate in the west and the Shan-Thai (or Sibumasu) continental plate in the east (Fig.3). The Sagaing Fault proper cuts through the eastern Tertiary sedimentary basin of Myanmar in a back-arc setting east of the (largely ordered) Central Magmatic Arc, a volcanic arc belt of Cretaceous to Miocene age (CMC,2005). In the northern part of the research area, the western splay of the Sagaing Fault cuts the eastern edge of the Wuntho Massif. The eastern margin of the eastern Tertiary basin is marked by the Shan Boundary Fault and the metamorphic core complex of the Mogok Belt, passing east into Paleozoic and Mesozoic sediments of the Shan-Thai Terrain. Within and east of the Sagaing Fault zone, older basement comprising Triassic and Permian carbonate, clastic rocks, and ophiolite slices is exposed in uplift, generally fault- controlled blocks unconformably overlain by younger sediments, predominantly of Tertiary age (CMC,2005).

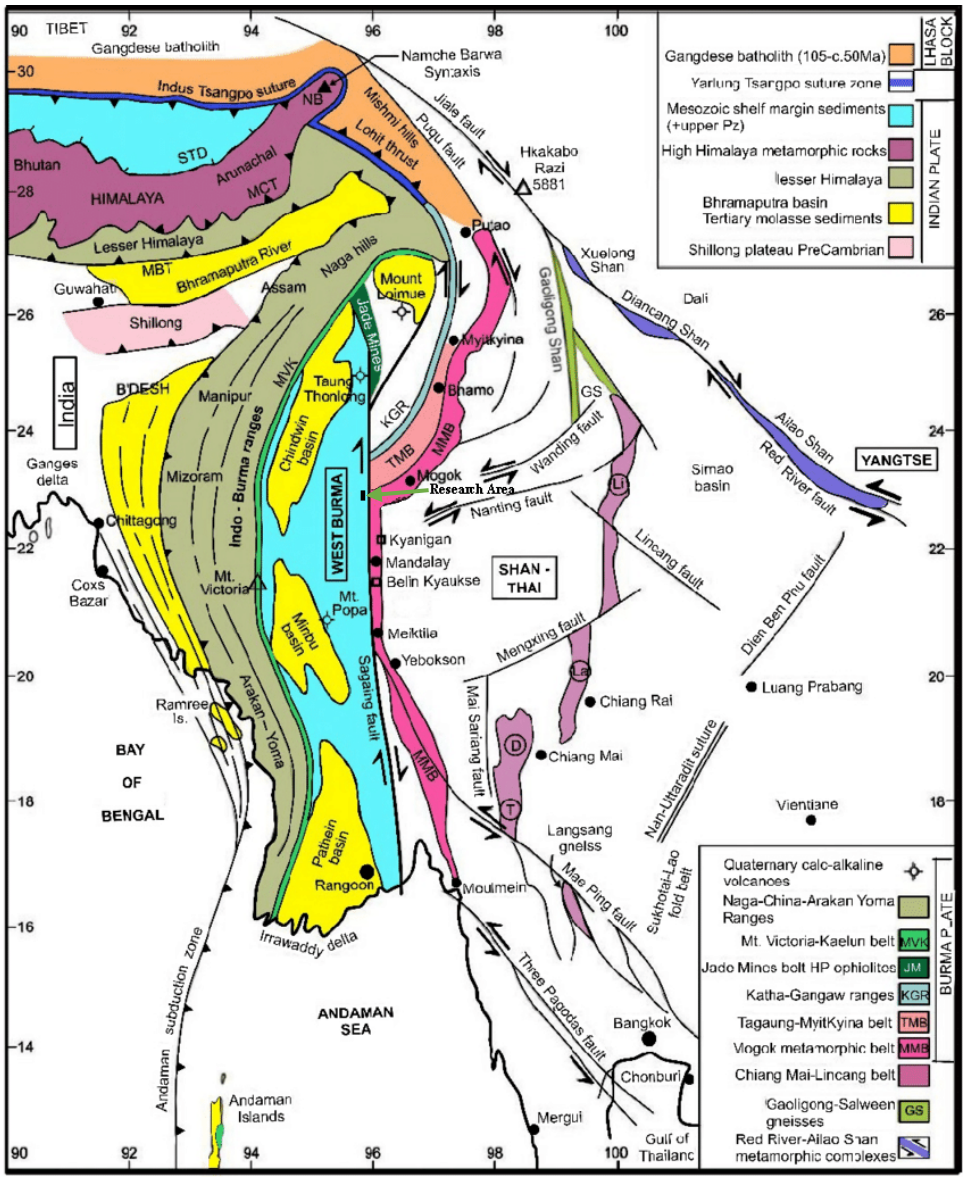

Figure (3): Regional geological map of Myanmar showing the principal tectonic units. (From Searle et al, 2007)

Local Geology

Permian and Triassic clastic and carbonate sediments occur as inliers, often partly structurally controlled, within younger sediments in the research area. The Taungzaw prospect is located within the Kyaukpahto-Zintaung inlier and it is a linear belt predominantly of Triassic carbonates and clastics of the Ngapyawdaw Chaung Formation that is sporadically exposed over more than 56km of strike and forms the Minwon Range. Aeromagnetic data indicated that the belt is continuous under shallow younger rock cover, where it is not exposed in the Taungzaw area. The carbonates include clean fossiliferous lithologies, but carbonaceous limestones have also been described. The Tertiary stratigraphy within the research area is not entirely clear. The Male Formation is dominated by very immature coarse feldspathic and lithic sandstones, often with a carbonate cement and with interbedded siltstones and mudstones, interpreted to be deposited in a continental to paralic setting.

The area was also subjected to compressional deformation in the middle to late Miocene, following the development of an aspreading center in the Andaman sea and the initiation of the Sagaing transform fault. This has resulteed in the open folding of the Male Formation sediments and the formation of the regional-scale dome which exposes the magmatic arc rocks of the Wuntho Massif. The study area lies in the continantal scale Sagaing Fault zone which comprises two main strands; an eastern fault along the course of the Ayeyarwady River (the Sagaing Fault) and a western one (the Kyauktan Fault), parallel to the main motorway in the western part of the area.

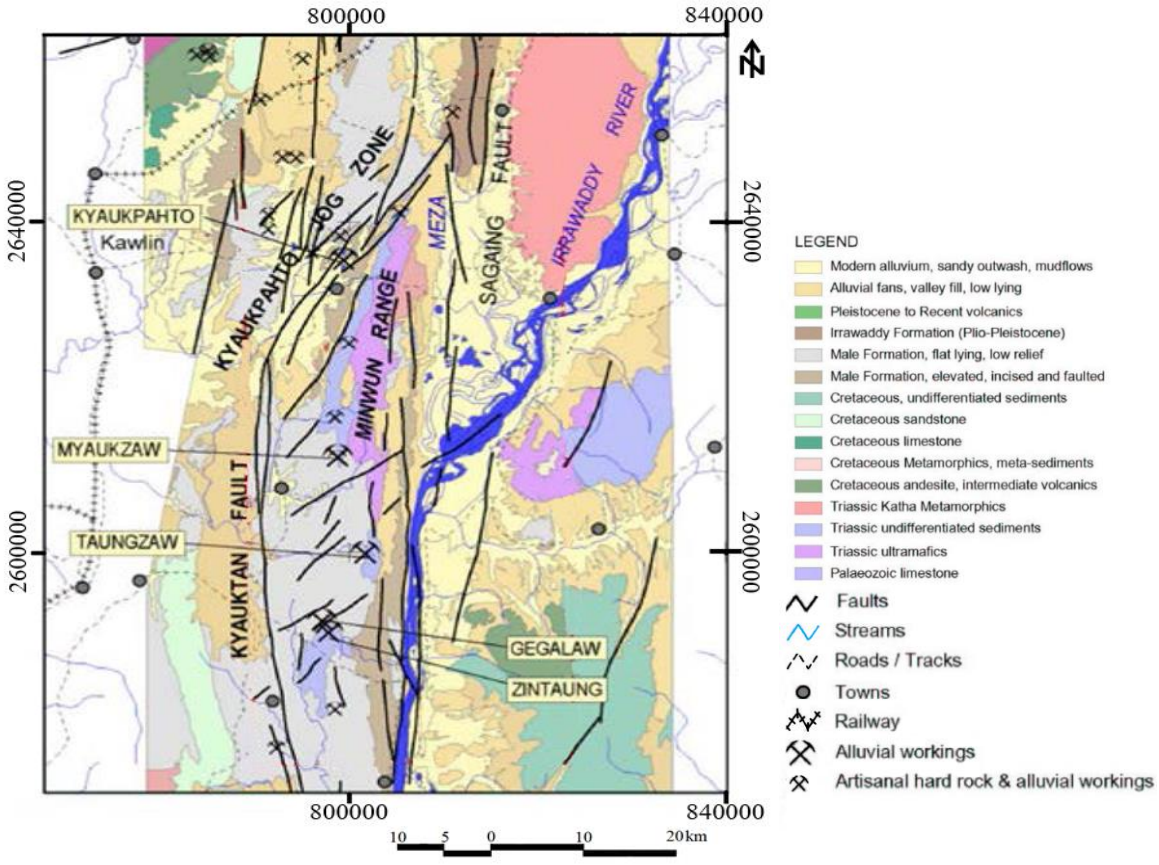

Figure (4): Geological and Structural map of Research Area. (CMC, 2005)

Mineralization

Gold mineralization in the Taungzaw area is localized within limited zones of silicification and quartz veinlet networks in sandstone and mudstone of the Male Formation (Fig.5). The mineralization appears to be closely associated with the NNE-SSW trending extensional fault, which is probably related directly to the dextral movement of the Sagaing Fault system. The halo around the zones of silicification and quartz veinlets is occupied by argillic alteration and decalcified zones of several tens of meters wide. Mineralization is associated with alteration characterized by quartz, chlorite, illite, and smectite mineral assemblages. Pyrite, sphalerite, and chalcopyrite are major primary sulfide minerals. Pyrite is the visible sulfide of the ore mineral in the sandstone host rock and hydrothermal breccia. Mineralized quartz veins occurrences and gold assay in quartz veins of Taungzaw adit are shown in (Figures 6. a, b).

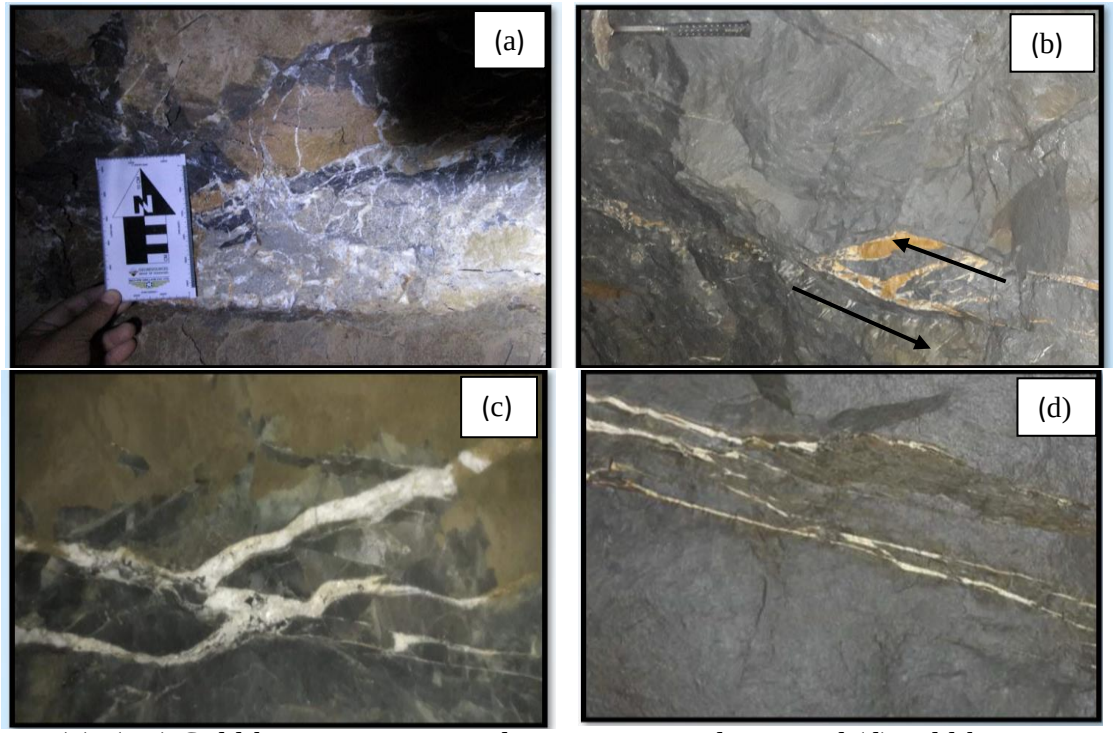

Figure (5): (a-c) Gold-bearing quartz veinlets occur in sandstone and (d) gold-bearing quartz veinlets in mudstone of Male Formation

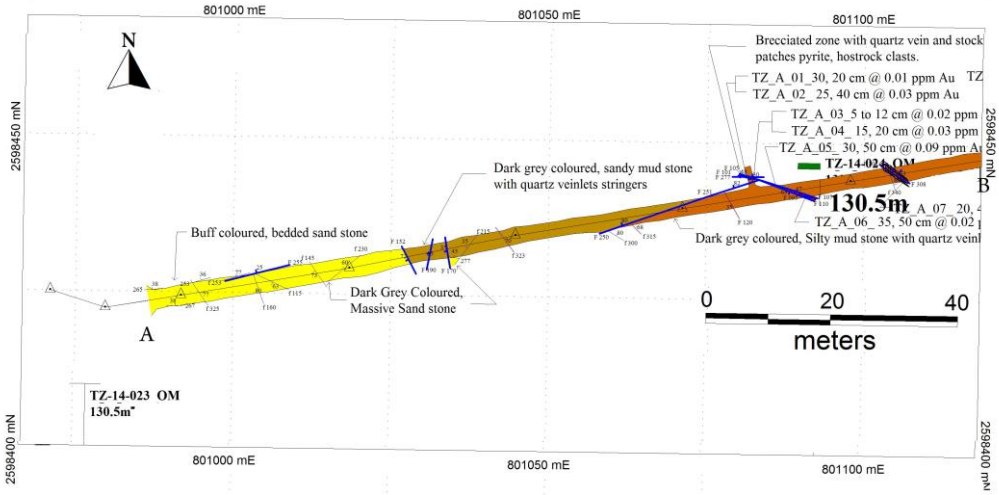

Figure (6): (a) Plan view of Mineralization quartz veins occurrences and gold assay in quartz veins of Taungzaw exploration adit along A-B

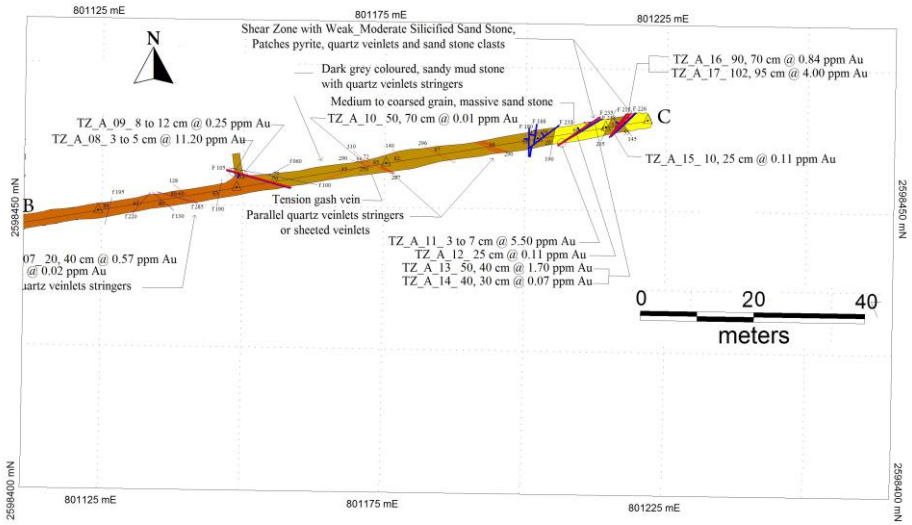

Figure (6): (b) Plan view of Mineralization quartz vein occurrences and gold assays in quartz veins of Taungzaw exploration adit along B-C

Fluid Inclusion Study

Quartz dominated mineralized samples were collected from the Taungzaw exploration adit, samples preparation was taken in Jabatan Geologi, Universiti Malaya by Dr. Jasmi, and Raman analysis was done by the Key Laboratory of Submarine Geosciences, SIO, Hangzhou, China.

Micro thermometry data of fluid inclusions were collected using a Linkam THMSG 600 (UK) heating-freezing stage with measurable temperatures ranging from −196 °C and 600 °C. The precision of the temperature measurement was ensured by calibration with the freezing point of pure water (0.0 °C) and the triple point of CO_2 (−56.6 °C). The accuracy of the temperature measurements was about ±0.1 and ±0.2 °C during freezing and heating respectively. The rate ranges for freezing and heating were adjusted between 10 and 20 °C/min but were gradually reduced to less than 0.2 °C/min when phase transitions were approached.

The Laser Raman analysis was carried out using a Renishaw Invia Raman micro spectrometry at the Key Laboratory of Submarine Geosciences, SIO, Hangzhou, China. Representative inclusions were chosen for analyzing the composition of the fluid inclusions. The spectral range fell between 200 and 5000 cm^{-1} and an argon laser light was used as a laser source with a wavelength of 514.4 nm at a laser power of 20 nw. The laser beam size was about 1 um in diameter with a wavenumber precision of +1 cm^{-1} and spectral resolution of +2 cm^{-1}. The settings of the instrument were kept constant throughout the analysis procedure.

Aqueous fluid inclusion salinities were calculated based on the ice-melting temperatures of the two-phase inclusion, whereas the salinities of aqueous-carbonic inclusion were estimated according to clathrate ice melting temperatures. The solid crystal (halite) dissolving temperatures were used to determine the salinities of solid-bearing inclusions. The total salinity of the fluid inclusions was expressed as wt.% NaCl equivalent.

The Nature of Fluid Inclusions

Primary, secondary, and pseudo-secondary inclusions were identified based on Roedder's criteria (1984), and primary inclusions were further classified according to their nature, number, phase proportion at room temperature, and phase transitions during cooling and heating, plus by laser Raman spectroscopy. Four types of inclusions were identified: type I(monophaseaqueous), type II (two phases liquid and vapor aqueous), type III (aqueouscarbonic) and type IV (liquid-rich aqueous). The photomicrographs of fluid inclusion are shown in (Fig. 7). The resume measurements of fluid inclusion are shown in table 1.

Type I Inclusions

Type I inclusions are rarely distributed and typically observed in pre-ore and occasionally in the sulfide ore stage. These inclusions are monophase H_2O, which are identified by laser Raman spectroscopy. The inclusions are ellipsoidal in shape, irregular, negative crystals, dark in colors, with sizes varying from 3 to 16 µm, but most of the inclusions have size of about 4 to 6 µm. Usually, these inclusions are observed as isolated forms and are rarely associated with types II and IV.

Type II Inclusions

Type II inclusions have two phases: aqueous liquid and vapor, but their volumetric ratios are approximately equal in most inclusions, and rarely vary between 20% (liquid) and 80% (vapor). This type is abundant in the pre-ore and the main sulfide ore stages. Inclusions sizes range from 1 to 22 µm, but are most commonly between 3 and 10 µm.

Type III Inclusions

Type III inclusions comprise three phases (i.e., $VCO_2 + LCO_2 + LH_2O$), but most of the inclusions are observed as two phases (i.e., $LCO_2 + LH_2O$) at room temperature. These inclusions occur as isolated patches in the pre-ore and sulfide ore stage I, which represents the primary origin and is occasionally observed with type II inclusions. Overall, their proportion is less than all other inclusion types. The type III inclusions can be further classified into two subtypes: IIIa and IIIb. Type IIIa inclusions have more H_2O than CO_2, while type IIIb inclusions contain more CO_2 than H_2O. Inclusion sizes range vary from 3 to 60 µm, however, most of them range from 10 to 20 µm. The shapes are typically oblate, elongated, negative crystals, and irregular. The volumetric proportions of CO_2 vary between 20 and 80%.

Type IV Inclusions

These types of inclusions consist of liquid and vapor phases, and are observed to occupy the highest inclusion population as compared with all other types, which is approximately up to 40%. These fluid inclusions are observed in all stages, however are most consistently found in the sulfide-ore stage II and late stages, as isolated or trial form along the growth zones, indicating a primary genesis. The range of size is observed from less than 2 µm to a maximum of 40 µm, and they are oblate, ellipsoidal, and irregular in shape. These inclusions contain an abundant ratio of vapor (approximately 30% to 40%) in the pre-ore and sulfide ore stage I, while the volumetric proportions of vapor are observed between 15–30 and 5–10% in the sulfide ore stage II and late stage, respectively.

Nature of fluid inclusions and their types

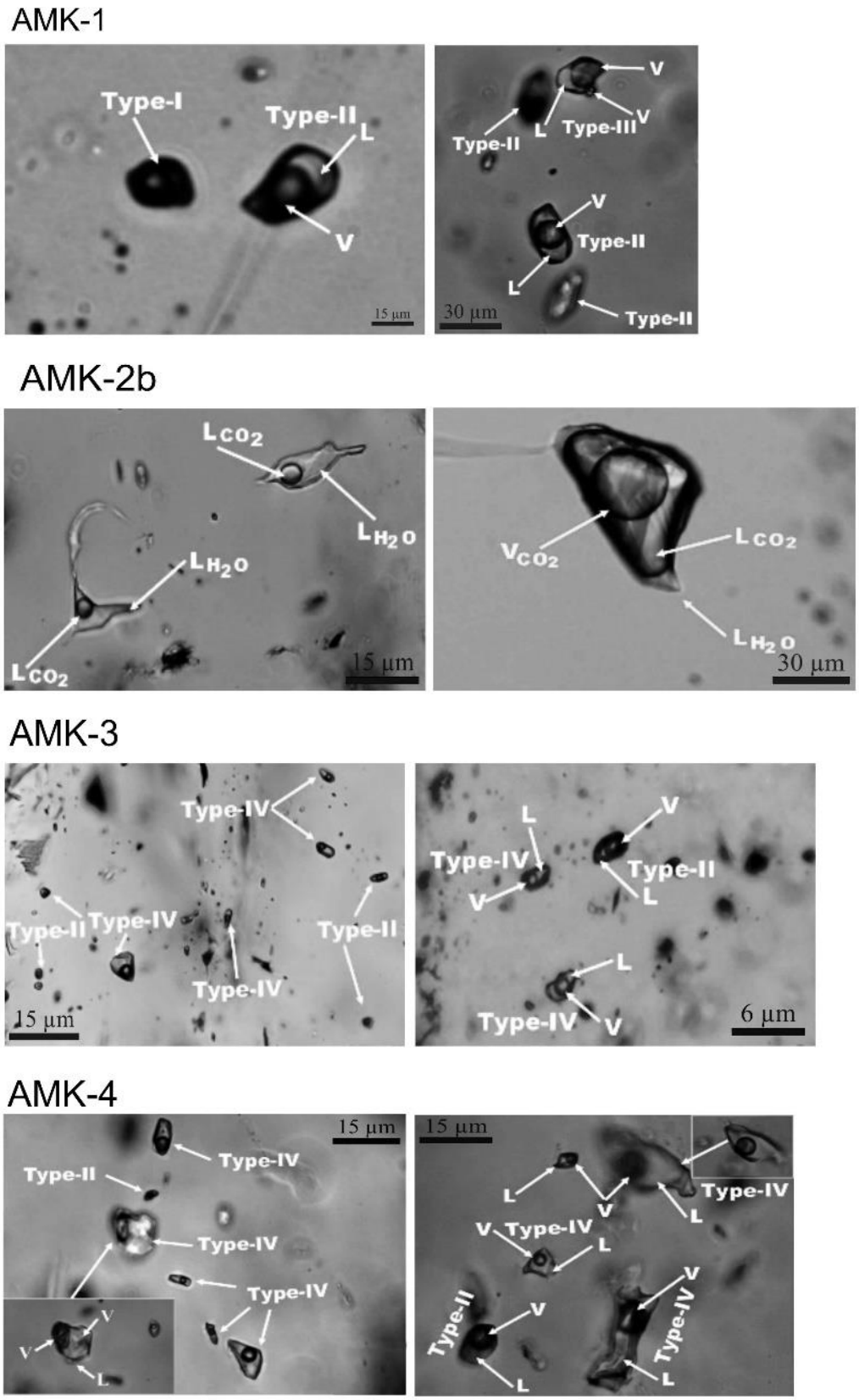

Figure (7): Photomicrographs of fluid inclusion from mineralized quartz vein samples

Table (1) Resume measurements of fluid inclusions.

Sample	Stage	Host Mineral	Type	Number	Size (μm)	Teu (°C)	Tm ice (°C)	Th (°C)	Salinity (wt.% NaCl eq.)
AMK-1	Sulfide ore	Quartz	II	7	2-27	-38.2	-9.7	171.2	1.61558
	Sulfide ore	Quartz	I			-56.1	-8.4	217.5	2.16338
	Sulfide ore	Quartz	II			-55.9	-13.6	211.2	2.43388
	Sulfide ore	Quartz	III			-59.4	-11.5	192.5	1.47168
	Sulfide ore	Quartz	II			-43.5	-5.4	162.2	0.710835
	Sulfide ore	Quartz	II			-44.3	-6.3	205.7	1.598978
	Sulfide ore	Quartz	IV			-52.4	-8.5	232.9	1.27862
AMK-2(a)	Sulfide ore	Quartz	II	7	1-15	-48.7	-12.2	254.4	2.14807
	Sulfide ore	Quartz	II			-46.1	-10.4	192.2	1.35788
	Sulfide ore	Quartz	IV			-37.8	-8.8	195.2	1.62073
	Sulfide ore	Quartz	II			-48.3	-7.9	196.7	1.5781
	Sulfide ore	Quartz	IV			-55.8	-7.6	234.2	2.21952
	Sulfide ore	Quartz	II			-44.3	-3.7	216.5	0.809116
	Sulfide ore	Quartz	II			-53.2	-7.3	188.6	0.85526
AMK-2(b)	Sulfide ore	Quartz	II	8	2-18	-56.5	-8.9	240.8	1.73359
	Sulfide ore	Quartz/Carbonate	IV			-59.3	-9.6	168.8	1.50733
	Sulfide ore	Quartz	II			-52.2	-2.3	219.8	0.866959
	Sulfide ore	Quartz	II			-59.6	-13.9	171.3	1.69801
	Sulfide ore	Quartz	II			-41.8	-3.9	235.2	2.302759
	Sulfide ore	Quartz/Carbonate	III			-37.9	-2.9	183.1	1.803863
	Sulfide ore	Quartz	II			-44.7	-2.2	223.9	1.708003
	Sulfide ore	Quartz/Carbonate	IV			-52.3	-3.1	242.9	2.109832
AMK- 3	Sulfide ore	Quartz	II	9	5-31	-46.2	-8.7	209.4	1.50729
	Sulfide ore	Quartz	IV			-43.1	-3.9	179.2	1.502759
	Sulfide ore	Quartz	IV			-42.7	-3.6	177.6	1.861155
	Sulfide ore	Quartz	II			-53.6	-8.9	232.9	1.73359
	Sulfide ore	Quartz	IV			-46.7	-11.3	254.4	2.2738
	Sulfide ore	Quartz/Carbonate	IV			-43.1	-6.3	205.7	1.598978
	Sulfide ore	Quartz	IV			-37.8	-8.1	195.2	1.81405
	Sulfide ore	Quartz	IV			-39.5	-7.9	191.3	1.5781
	Sulfide ore	Quartz	IV			-55.1	-9.5	245.3	2.39851
AMK- 4	Sulfide ore	Quartz	II	11	2-24	-52.1	-9.1	235.2	1.95754
	Sulfide ore	Quartz	IV			-50.7	-2.8	221.7	1.649699
	Sulfide ore	Quartz/Carbonate	IV			-49.4	-14.6	256.3	2.29979
	Sulfide ore	Quartz	II			-39.6	-8.2	193.7	1.9311

	Sulfide ore	Quartz	IV			-46.8	-7.4	197.3	0.97732
	Sulfide ore	Quartz	II			-87.9	-12.8	173.7	1.71039
	Sulfide ore	Quartz	IV			-56.9	-10.2	252.7	2.2534
	Sulfide ore	Quartz	IV			-43.2	-9.3	201.6	0.72426
	Sulfide ore	Quartz/Carbonate	IV			-54.8	-7.7	216.1	1.612115
	Sulfide ore	Quartz	II			-48.6	-12.9	198.2	1.69567
	Sulfide ore	Quartz	IV			-47.7	-12.2	233.9	2.45385

Teu eutectic temperature (First melting temperature)
Tm ice final ice melting temperature
Th homogenization temperature of fluid inclusion

The Salinity of hydrothermal fluid

Fluid inclusion is calculated from the melting temperature. The salinity value ranges from 0.71 to 2.45 wt % NaCl eq. and the average salinity is 1.69 wt.% NaCl eq. (Fig. 8). Based on the epithermal system's average homogenization temperature ranges (210 ºC) and the averaging salinity is of 1.69 wt.% NaCl eq. (Wilkinson, 2001). The salinity variations are controlled by fluid mixing.

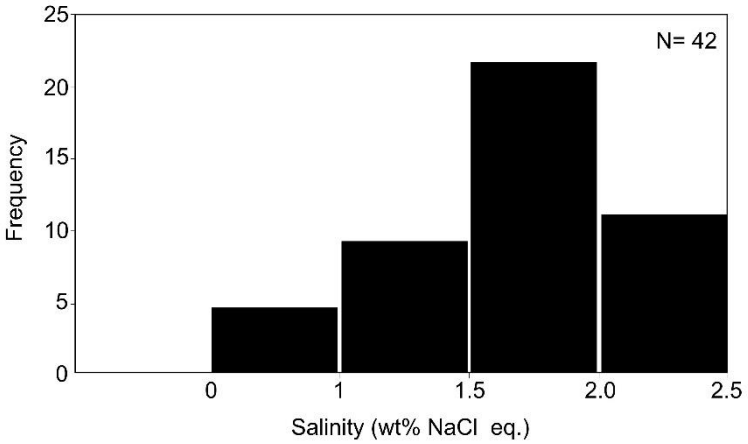

Figure (8): Frequency distribution of Salinity (wt% NaCl eq.) of hydrothermal fluid.

Homogenization temperature of fluid inclusion

Based on the fluid inclusion data, the homogenization temperature of the Gegalaw and Taungzaw areas is 162 °C - 256 °C. The distribution of homogenization temperatures of fluid inclusions (histograms) is shown in (Fig. 9). According to the homogenization temperature of the histogram, the formation temperature at shallow depth is 200 °C to 220 °C. The measurement of the melting temperature of fluid inclusion data ranges from -2.2 °C to -4.6 °C.

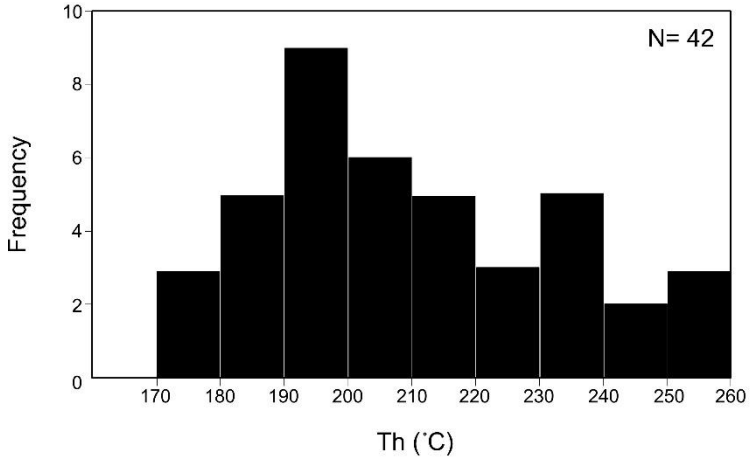

Figure (9): Frequency distribution of homogenization temperatures (Th) of fluid inclusions.

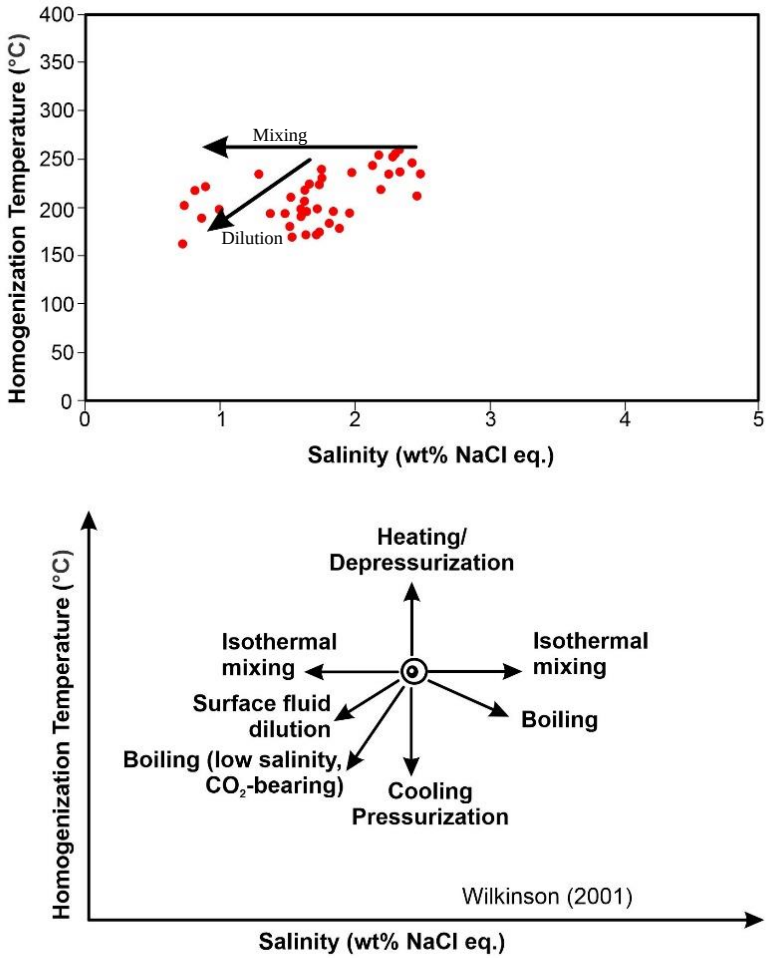

Figure (10): Correlation binary plot diagram of salinity (wt.% NaCl eq..) versus homogenization temperatures (Th, ºC) for fluid inclusions of the Taungzaw deposit area (Wilkinson, 2001)

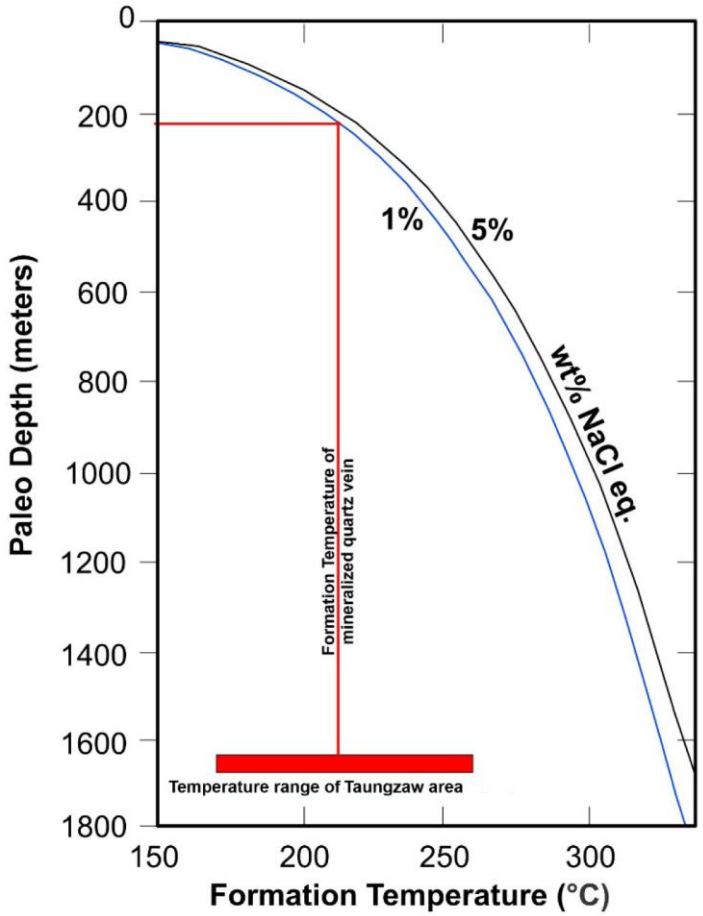

Figure (11): Estimation of the formation depth of mineralization quartz vein samples from the Taungzaw area by using the boil point curve of (Hass, 1971).

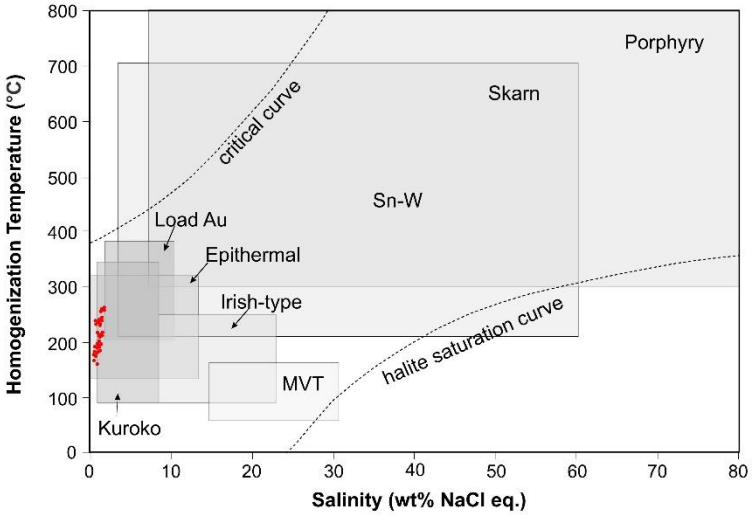

Figure (12): Homogenization temperature (Th ºC) versus salinity diagram illustrating typical ranges for inclusions from different mineral deposit types (Wilkinson, 2001) and micro thermometric data of fluid inclusions from the Taungzaw area in the epithermal field.

Conclusion

In the Taungzaw area, gold and base metal mineralization is mainly hosted by sedimentary rocks. Mineralization takes the form of open space filling veins, stock works, and on rare occasion, disseminated nature. The gold-bearing quartz veins consist of pyrite, chalcopyrite and arsenopyrite. Hydrothermal fluid altered the mineralized host rocks in the process of silicification, decalcification and argillic assemblages. Based on the fluid inclusions study, the Taungzaw area was not observed for boiling fluid evidence. It is possibly related to the isothermal fluid mixing and surface fluid dilution processes (Fig. 10). The formation temperature of mineralized quartz veins can be estimated from the fluid inclusion micro thermometric data and the formation depth can be projected from the boiling point curve of (Hass, 1971) (Shepherd et al., 1985). The formation temperature is plotted on the temperature axis and the salinity value is plotted on the salinity curves (Fig. 11). According to the plotting data (Fig. 12), the study area fits into the epithermal environment (Wilkinson, 2001). From the combination of available data from fluid inclusion types, micro thermometric measurement, formation temperature of mineralized quartz vein, associated characteristics of hydrothermal alteration types, and paleo-depth, it can be concluded that the hydrothermal system of the Taungzaw prospect was developed under the epithermal condition.

References

CMC,2005. Exploration Report of Care Mineral Corporation, Switzerland, unpublish report.

Gardiner, N.J., Robb, L.J., Searle, M.P., The metallogenic provinces of Myanmar, *Apply Earth Science 2014, vol.123, No.1.*

Hass, J.L., 1971. The Effect of Salinity on the Maximum Thermal Gradient of a Hydrothermal System at Hydrostatic Pressure, *Economic Geology* 66, 940946.

Roedder, E., 1984. Fluid inclusions, Mineralogical Society of America, *Review in Mineralogy* 12, 646.

Shepherd, T.J., 1985. A Practical Guide to Fluid Inclusion Studies, Balckie, p. 237.

White, N.C., and Hedenquist, J.W., 1995. Epithermal gold deposits: Styles, characteristics and exploration: SEG Newsletter, p 1-13.

Wilkinson, J.J., 2001. Fluid inclusions in hydrothermal ore deposits, *Lithos* 55, 229272.

Ye Myint Swe, Khin Zaw and Than Htay 2004a.Sedimentary rock-hosted gold mineralization along the Sagaing Fault Zone. *International Symposium on the Geological Evolution of East and Southeast Asia*, February 2004, Bangkok, Thailand, 67-68.